Nanoscale Advances

ROYAL SOCIETY OF CHEMISTRY

PAPER

View Article Online
View Journal | View Issue

Cite this: *Nanoscale Adv.*, 2022, **4**, 1345

Ligand-assisted deposition of ultra-small Au nanodots on Fe_2O_3/reduced graphene oxide for flexible gas sensors†

Jian Wang,[a] Essalhi Fatima-Ezzahra,[a] Jie Dai,[a] Yanlei Liu,[a] Chengjie Pei,[a] Hai Li,[a] Zhiwei Wang*[ab] and Xiao Huang*[a]

Received 9th October 2021
Accepted 17th January 2022

DOI: 10.1039/d1na00734c

rsc.li/nanoscale-advances

The development of flexible room-temperature gas sensors is important in environmental monitoring and protection. In this contribution, by using 1-octadecanethiol (ODT) as a surface ligand, Au nanodots (NDs) with ultra-small size of ~1.7 nm were deposited on the surface of α-Fe_2O_3/reduced graphene oxide (rGO). The Au ND–ODT/α-Fe_2O_3/rGO composite was fabricated into flexible gas sensors, which could detect NO_2 gas down to 200 ppb at room temperature. Compared with α-Fe_2O_3/rGO, Au ND–ODT/α-Fe_2O_3/rGO showed enhanced sensing performance because of the beneficial effects of Au NDs, including facilitating the adsorption of NO_2 molecules and forming ohmic-like contact with rGO and α-Fe_2O_3. In addition, the sensing performance of the composite was also influenced by the surface ligands of the Au NDs. Ligands with less polar terminal groups were found to be beneficial to charge transfer in the sensing film. Moreover, Au ND–ODT/α-Fe_2O_3/rGO-based flexible sensors showed negligible performance deterioration under moderately bent conditions, suggesting their potential to be used in portable and wearable devices.

1. Introduction

The fast technological and industrial development has led to increasingly serious air pollution. Among the several gaseous pollutants in air, nitrogen dioxide (NO_2), which is usually produced by fuel burning and vehicle exhausts,[1] can cause several pulmonary diseases such as pulmonary edema, tracheitis and pneumothorax, and is also the main cause for acid rain. Therefore, the development of highly sensitive and selective NO_2 gas sensors is important to environmental monitoring and protection.[2,3] In addition, making gas sensors flexible can enable their integration into portable and wearable devices.[4,5]

Metal oxides (MOXs), such as ZnO,[6–8] NiO,[9–11] Fe_2O_3,[12–14] and In_2O_3 (ref. 15–17) have been widely used for detection of hazardous gases over the past few decades. For example, alpha-iron oxide (α-Fe_2O_3) is a commonly used sensing material for detection of acetone,[18] H_2S[19] and NO_2 (ref. 14) because of its low cost and simple production.[20] However, gas sensors based on MOXs normally require high operating temperatures due to their poor conductivity and moderate surface activity at room temperature (RT), making it difficult to fabricate RT gas sensors with simple configurations towards flexible devices.

Hybridization of MOXs with conductive materials such as graphene derivatives[21,22] and carbon nanotubes[23,24] can improve their gas sensing performances. For instance, reduced graphene oxide (rGO), which possesses excellent electrical conductivity, large specific surface area, and good surface activity, has been wildly utilized to composite with MOXs for gas sensing.[25–27] Examples of MOX/rGO-based sensing materials include ZnO/rGO,[28] Fe_2O_3/rGO,[29] and CuO/rGO[30] for enhanced H_2S, NO_2, and acetone detection, respectively. Introducing noble metal nanostructures in sensing materials is another strategy to improve the gas sensing performance of MOX-based gas sensors. This is because, in addition to their good conductivity, noble metal nanomaterials can provide lower energy required for adsorption of gas molecules based on both experimental and theoretical investigations.[31] For example, noble metals such as platinum (Pt),[32] gold (Au),[33] silver (Ag)[34] and palladium (Pd)[35] have been used to improve the gas sensing response of MOX-based sensors. Besides, previous reports have suggested that the type of surface ligands can influence the surface activity of noble metal nanostructures.[2,36] However, few studies have investigated the ligand effects of metal nanomaterials in gas sensing.

In this work, a composite material, *i.e.* Au ND–ODT/α-Fe_2O_3/rGO, containing ultra-small Au nanodots (NDs) functionalized with 1-octadecanethiol (ODT), α-Fe_2O_3 and rGO was prepared

[a]*Institute of Advanced Materials (IAM), Nanjing Tech University (Nanjing Tech), 30 South Puzhu Road, Nanjing 211816, China. E-mail: iamxhuang@njtech.edu.cn*

[b]*Frontiers Science Center for Flexible Electronics, Xi'an Institute of Flexible Electronics (IFE), Xi'an Institute of Biomedical Materials & Engineering, Northwestern Polytechnical University, 127 West Youyi Road, Xi'an 710072, China. E-mail: iamzwwang@nwpu.edu.cn*

† Electronic supplementary information (ESI) available: Fig. S1–S12. See DOI: 10.1039/d1na00734c

and applied in NO_2 gas sensing at RT, showing enhanced performance as compared with α-Fe_2O_3/rGO-based sensor. The improved sensing performance was attributed to the Au NDs, which facilitated the adsorption of NO_2 gas and formed the ohmic-like contact with rGO and α-Fe_2O_3. The surface ligands of Au NDs were also found to influence the sensing performance. Flexible gas sensors based on Au ND–ODT/α-Fe_2O_3/rGO exhibited well-maintained responses under bent conditions due to the good mechanical strength, flexibility and film-forming ability of rGO.

2. Materials and methods

2.1. Materials

Graphene oxide (GO) aqueous solution (0.5 g L^{-1}) was commercially purchased from Shanghai Carbon Source Huigu New Material Technology Co., Ltd, China. $FeCl_3 \cdot 6H_2O$ was purchased from Shanghai Adamas Reagents Co., Ltd, China. $HAuCl_4 \cdot H_2O$ was purchased from Beijing Huawei Ruike Chemical Co., Ltd, China. 1-Octadecanethiol (ODT) and 16-mercaptohexadecanoic acid (MHA) were purchased from Shanghai Aladdin Biochemical Technology Co., Ltd, China. Ethanol (99.7%) was purchased from Sinopharm Chemical Reagent Co., Ltd, China. Printable Ag ink was purchased from Shanghai Mifang Electronic Technology Co., Ltd, China. All chemicals were used without further purification.

2.2. Preparation of α-Fe_2O_3/rGO hybrids

Typically, 0.25 mmol $FeCl_3 \cdot 6H_2O$ was mixed with 40 mL GO aqueous solution (0.5 g L^{-1}) under stirring for 10 min. This mixture was further ultra-sonicated for 20 min before being added into a 50 mL Teflon-lined stainless-steel autoclave and then heated at 160 °C for 18 h. After being naturally cooled to room temperature (RT), the solution was centrifuged and washed with deionized water for 3 times and re-dispersed in 10 mL ethanol for further use.

2.3. Preparation of Au/α-Fe_2O_3/rGO hybrids

To decorate Au nanodots (NDs) on α-Fe_2O_3/rGO, 2 mL of the above-mentioned α-Fe_2O_3/rGO dispersion, 1 mL $HAuCl_4$·ethanol solution (1 mg mL^{-1}), 2 mL ODT (or MHA) ethanolic solution (1 mg mL^{-1}) and 8 mL ethanol were mixed in a 20 mL glass bottle, which was irradiated with a 150 W xenon lamp for 2 min. The solution was then centrifuged at 7000 rpm and washed twice with ethanol. Depending on the ligand used, the products were named as Au ND–ODT/α-Fe_2O_3/rGO hybrids or Au ND–MHA/α-Fe_2O_3/rGO hybrids.

2.4. Materials characterization

Transmission electron microscopy (TEM, JEOL, 2100Plus and 2100F, Japan) was used to investigate the morphologies and microstructures of the samples. X-ray diffraction (XRD, Rigaku, XtaLAB mini II, Japan) was performed with Cu Kα radiation (λ = 1.54 Å). An X-ray photoelectron spectrometer (XPS, VersaProbe, PHI 5000, Japan) was utilized to analyze the oxidation state of the GO, and all the binding energies were calibrated to the C 1s band at 284.6 eV. An ultraviolet photoelectron spectrometer (UPS, VersaProbe, PHI 5000, Japan) coupled with an ultraviolet and visible spectrophotometer (UV, Shimadzu, UV-1780, Japan) was used to measure the electronic work functions and band levels of different materials.

2.5. Fabrication of flexible gas sensors and gas sensing tests

By employing a microelectronic printer (Shanghai Mifang Electronic Technology Co., Ltd, Scientific 3, China) with commercial Ag ink, arrays of interdigitated Ag electrodes were printed on polyethylene terephthalate (PET) substrates. To fabricate the flexible gas sensors, 20 μL of the sensing material solution was spin-coated on the as-prepared interdigitated Ag electrodes and then dried at RT for 2–3 h.

The gas sensing tests were conducted at RT in a sealed chamber. Constant currents were applied to the sensor electrodes and the variation of resistance was recorded using a data acquisition system (34972A, Agilent). The response of the sensor was defined as $\Delta R/R_0$ (%) ($\Delta R = R_g - R_0$, in which R_0 and R_g are the resistances of the sample in simulated air environment (20.9% O_2, 79.1% N_2, and 19% RH) and the target gas, respectively). The sensor response and recovery times refer to the times when the sensor reaches 90% of the total resistance change during the response and recovery process, respectively.

3. Results and discussion

The preparation process of Au nanodot (ND)–1-octadecanethiol (ODT)/α-Fe_2O_3/reduced graphene oxide (rGO) hybrid is schematically illustrated in Fig. 1a. Typically, α-Fe_2O_3 nanoparticles (NPs) with a size of 30–40 nm were first deposited on GO nanosheets *via* a hydrothermal reaction, during which GO was also reduced to rGO because of the reducibility of H_2O under high temperature and pressure[29,37] (see Fig. S1 and S2 in the ESI†). After that, by using ODT as a surface ligand, Au NDs were decorated on the as-prepared composite through a photochemical reaction.[38] As shown in Fig. 1b and S3a (see in the ESI†), Au NDs with an average size of ~1.7 nm were well dispersed on the surface of α-Fe_2O_3/rGO. The ultra-small size of the Au NDs was achieved due to the strong binding of the ODT molecules to Au surfaces, which prevented the Au nanoparticles from growing large. Energy dispersive X-ray (EDX) mapping of a typical composite reveals the distribution of Au, Fe and C elements (Fig. 1c). The structure properties of Au ND–ODT/α-Fe_2O_3/rGO were investigated with X-ray diffraction (XRD), high resolution transmission electron microscope (HRTEM) analysis and selected area electron diffraction (SAED). The XRD pattern of the composite (see Fig. S3b in the ESI†) is similar to that of α-Fe_2O_3/rGO without showing the characteristic peaks for Au, which is due to the ultra-small size of the Au NDs based on Scherrer's theory.[39,40] As shown in the HRTEM image in Fig. 1d, lattice spacings of 0.17 and 0.23 nm can be observed, which can be assigned to the (116) planes of α-Fe_2O_3 and (111) planes of Au, respectively. Besides, the SAED pattern of the product also reveals rings for rGO and α-Fe_2O_3 (Fig. 1e).

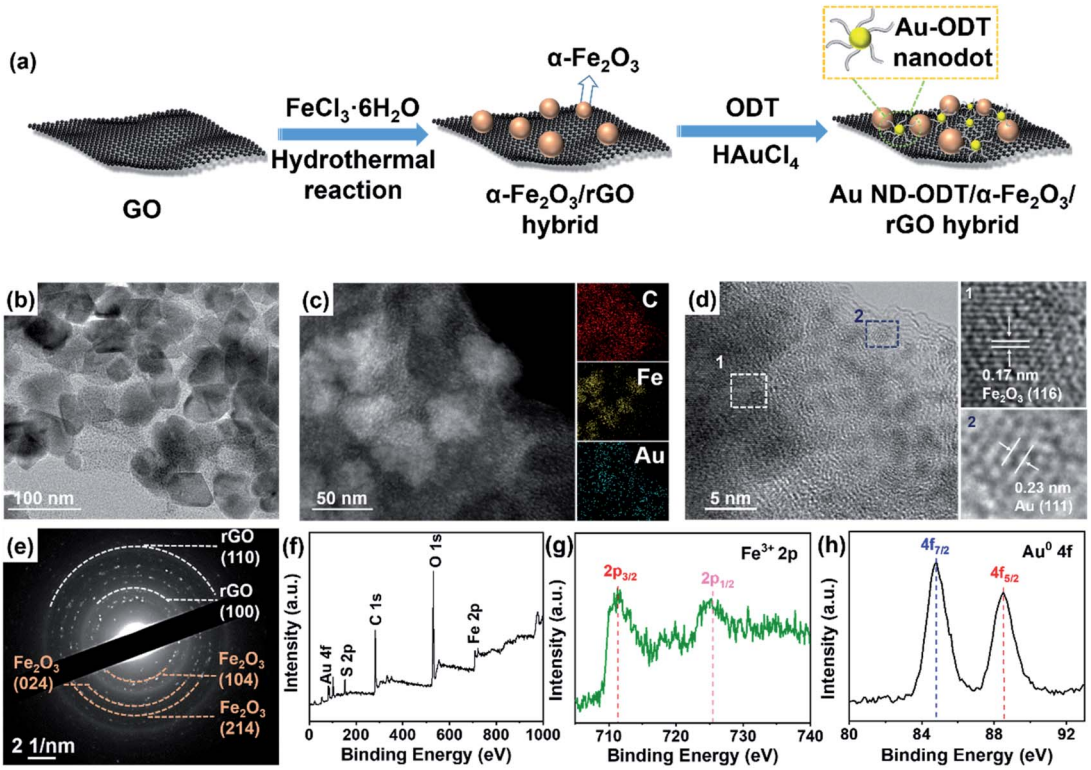

Fig. 1 (a) Schematic illustration of the preparation of Au ND–ODT/α-Fe_2O_3/rGO hybrids. (b) TEM image, (c) STEM image and EDX mapping, (d) HRTEM image, (e) SAED pattern, (f) XPS full scan spectrum, (g) high-resolution Fe 2p spectrum and (h) Au 4f spectrum of the Au ND–ODT/α-Fe_2O_3/rGO composite.

The oxidation states of the as-prepared Au ND–ODT/α-Fe_2O_3/rGO were investigated by X-ray photoelectron spectroscopy (XPS). The survey spectrum of the sample shows the presence of Au, Fe and C elements (Fig. 1f). The high-resolution Fe 2p spectrum shows a doublet at 711.7 and 725.6 eV, corresponding to the $2p_{3/2}$ and $2p_{1/2}$ bands of Fe^{3+}, respectively (Fig. 1g).[41] Besides, in the Au 4f spectrum, two peaks at binding energies of 84.8 and 88.5 eV can be assigned to the Au $4f_{7/2}$ and $4f_{5/2}$ bands of Au^0, respectively (Fig. 1h), indicating the successful photochemical reduction of Au^{3+}.[42]

The as-prepared composites, namely, α-Fe_2O_3/rGO and Au ND–ODT/α-Fe_2O_3/rGO were spin-coated onto interdigitated Ag electrodes which were inkjet-printed on flexible polyethylene terephthalate (PET) substrates (Fig. 2a) to prepare flexible gas sensors. The response–recovery curves of these gas sensors toward NO_2 were studied at RT in simulated air (20.9% O_2, 79.1% N_2, and 19% RH) with target gas concentrations increasing from 200 to 1000 ppb (Fig. 2b). All of the sensors showed decreased resistance upon NO_2 exposure, and the reduction in resistance (ΔR) increased with increasing NO_2 concentrations (Fig. 2b). The α-Fe_2O_3/rGO and Au ND–ODT/α-Fe_2O_3/rGO sensors both exhibited fast response times (*e.g.*, about tens of seconds to 800 ppb NO_2) but slow recovery times (*e.g.*, more than 20 minutes to 800 ppb NO_2) (see Fig. S4 in the ESI†). This points to the strong interaction between the NO_2 molecules and the sensing material, leading to a slow desorption process.[43–45] In our sensing materials, the rGO nanosheets and α-Fe_2O_3 showed p-type and n-type semiconducting properties, respectively, based on their ultraviolet photoelectron spectroscopy (UPS) and ultraviolet-visible (UV-vis) spectroscopy analysis results (see Fig. S5 and S6 in the ESI†).

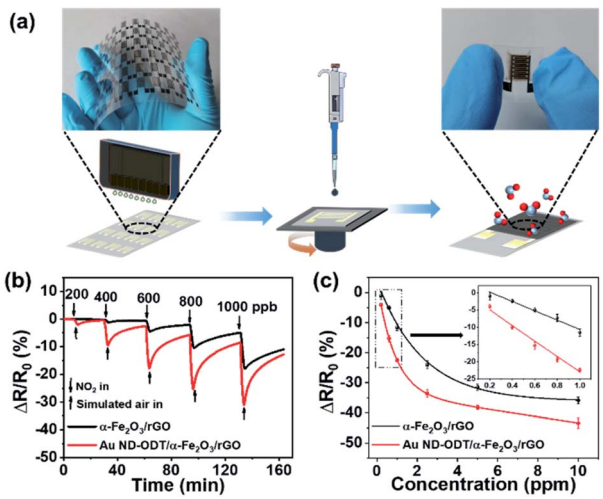

Fig. 2 (a) Schematic illustration of the preparation of the flexible NO_2 sensor, with photographs of the printed Ag electrode array and flexible gas sensor coated with Au ND–ODT/α-Fe_2O_3/rGO. (b) Dynamic response–recovery curves of α-Fe_2O_3/rGO and Au ND–ODT/α-Fe_2O_3/rGO in response to NO_2 gas with different concentrations at RT. (c) Responses of α-Fe_2O_3/rGO and Au ND–ODT/α-Fe_2O_3/rGO sensors for NO_2 with different concentrations.

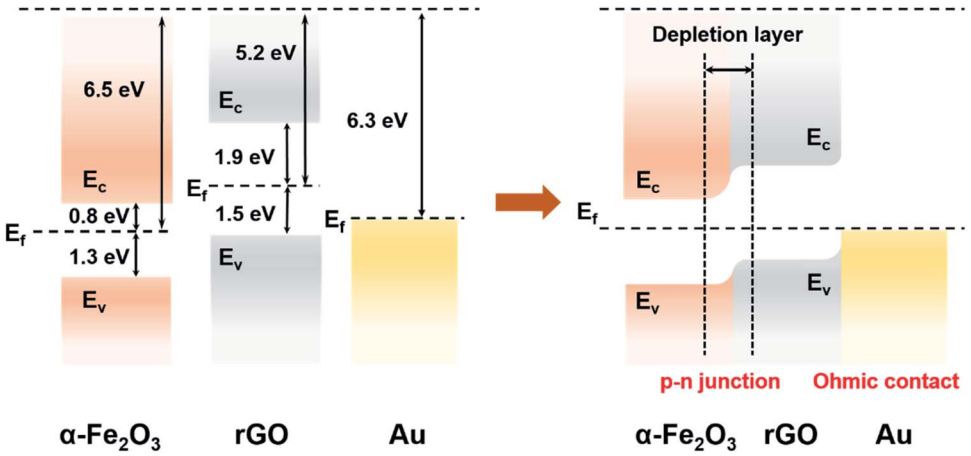

Fig. 3 Schematic of the band level diagram of the Au ND–ODT/α-Fe_2O_3/rGO composite.

Generally, NO_2, as an oxidizing gas, could extract electrons from sensing materials. This increased the concentration of holes in the p-type rGO, which was the main conducting matrix in the hybrid sensing material. The n-type α-Fe_2O_3 also lost electrons to NO_2, and because of its lower Fermi level than that of rGO (Fig. 3), its electron vacancies were compensated by extracting electrons from rGO. This further increased the hole concentration in rGO, thus decreasing the resistance of the sensing film.[46] Moreover, with the work functions, bandgaps and band level positions determined with UPS and UV-vis spectrometers (see Fig. S5 and S6 in the ESI†), we also studied the band alignment in the composite material as shown in Fig. 3. It can be seen that a p–n junction might form between rGO and α-Fe_2O_3, resulting in a charge neutral interface (the depletion layer). The adsorption of NO_2 molecules could narrow the width of the depletion layer and facilitate the charge transfer at the heterojunction, thus resulting in further decreased resistance of the sensing film.[47–50]

The Au ND–ODT/α-Fe_2O_3/rGO-based sensor showed an enhanced sensing performance as compared with the α-Fe_2O_3/rGO sensor, for example, with at least three times higher response at 200 ppb (Fig. 2c). Such an improvement might be attributed, in part, to the increased gas adsorption sites on the ultra-small Au NDs. Besides, due to the lower work function of Au NDs as compared to that of rGO, an ohmic contact might be established between them (Fig. 3), which favoured the charge transfer from rGO to Au NDs and finally to the NO_2 molecules, thus improving the sensitivity of the hybrid sensing material.[51,52] Moreover, ohmic like contact might also form between α-Fe_2O_3 and Au NDs (see Fig. S7 in the ESI†), which enabled facile electron transfer across the Au/α-Fe_2O_3 interface, leading to the formation of additional electron vacancies in α-Fe_2O_3 and thus an enhanced sensitivity. In addition, our Au ND–ODT/α-Fe_2O_3/rGO-based sensor exhibits performance comparable to that of many previously reported RT NO_2 gas sensors (see Table S1 in the ESI†)[53–61] and outperforms the recently reported rGO nanofiber,[54] Au–CuO[59] and MoS_2 (ref. 60) based sensors.

Since ODT molecules were used as the capping agent to prepare the ultra-small Au NDs, we also investigated the effect of surface ligands on the gas sensing performance by using another type of thiol, *i.e.* 16-mercaptohexadecanoic acid (MHA), to prepare Au NDs (see Fig. S8 and S9 in the ESI†), and the resulting material was denoted as Au ND–MHA/α-Fe_2O_3/rGO. Our results showed that the Au ND–ODT/α-Fe_2O_3/rGO-based sensor outperformed the Au ND–MHA/α-Fe_2O_3/rGO sensor (see Fig. S10 in the ESI†). This was mainly attributed to the different terminal groups of the two types of thiols (*i.e.* carboxylic acid groups in MHA and methyl groups in ODT), considering their similar alkane chain lengths. Compared to the less polar methyl groups of ODT molecules, the polar carboxylic acid groups of MHA possess higher electron withdrawing ability which could extract electrons from Au NDs,[62] and hinder the charge transfer in the sensing film (Fig. 4). This was proved by the lower baseline resistance of the Au ND–ODT/α-Fe_2O_3/rGO sensor compared to that of the Au ND–MHA/α-Fe_2O_3/rGO sensor (see Fig. S10 in the ESI†).

The selectivity of Au ND–ODT/α-Fe_2O_3/rGO-based sensors was studied by comparing their responses to NO_2 with other

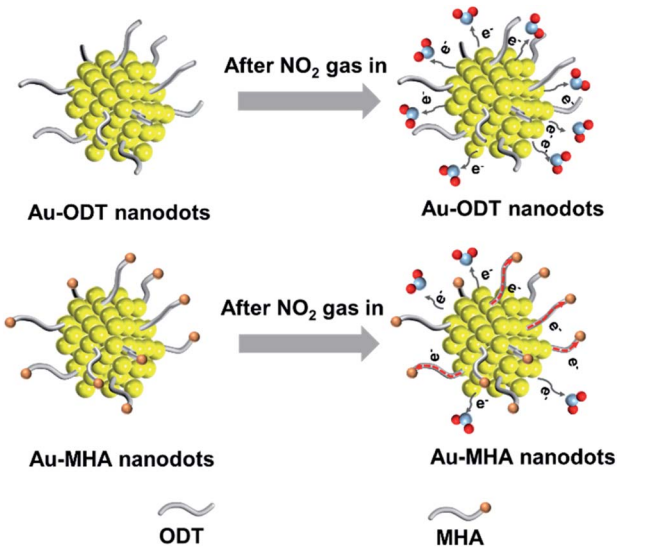

Fig. 4 Schematic illustration of the effect of surface ligands of Au NDs on gas sensing.

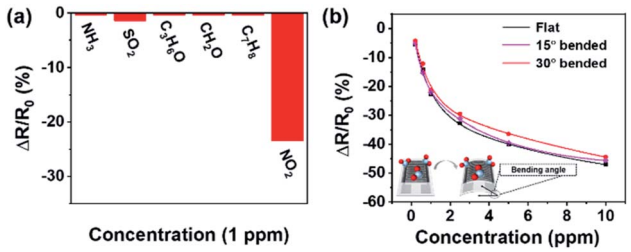

Fig. 5 (a) Responses of the Au ND–ODT/α-Fe_2O_3/rGO sensor to 1 ppm of NH_3, SO_2, C_3H_6O, CH_2O, C_7H_8 and NO_2. (b) Comparison of the responses of a typical Au ND–ODT/α-Fe_2O_3/rGO sensor to NO_2 under flat and different bent conditions.

gases including NH_3, SO_2, acetone, formaldehyde and methylbenzene. The responses to the other gases were at least 8 times lower than that to NO_2, indicating the good selectivity of the hybrid sensing material (Fig. 5a). Lastly, we demonstrated that our sensors on flexible substrates can work under bent conditions. As shown in Fig. 5b, a typical gas sensor showed similar sensing responses under the flat and bent conditions at bending angles of 15° and 30°, and negligible performance change even after the device was bent 300 times (see Fig. S11 in the ESI†). This can be due to the good mechanical strength, flexibility and film-forming ability of rGO sheets, which could help to avoid the loss of contact points under moderately bent conditions. However, at larger bending angles, *e.g.* 45° and 60°, the loss of contact points in the sensing film might occur, causing performance deterioration (see Fig. S12 in the ESI†).

4. Conclusion

In summary, the Au ND–ODT/α-Fe_2O_3/rGO composite was successfully prepared, which was utilized for NO_2 sensing. The sensor could detect NO_2 with concentrations down to 200 ppb at RT in simulated air, and showed improved sensing performance as compared with α-Fe_2O_3/rGO because of the advantageous effects of Au NDs. Besides, the surface ligands on Au NDs also influenced the sensing performance, that is, less polar terminal groups of the ligands favored charge transfer in the sensing film. Flexible gas sensors based on Au ND–ODT/α-Fe_2O_3/rGO exhibited well-maintained sensing responses under moderately bent conditions, indicating their potential applications in portable and wearable electronic devices.

Conflicts of interest

The authors declare no competing interests.

Acknowledgements

This work was supported by the National Natural Science Foundation of China (grant no.: 51832001), the Fundamental Research Funds for the Central Universities of China, the Young 1000 Talents Global Recruitment Program of China, the Joint Research Funds of Department of Science & Technology of Shaanxi Province and Northwestern Polytechnical University (grant no.: 2020GXLH-Z-026 and 2020GXLH-Z-027), and the China Postdoctoral Science Foundation (grant no.: 2021M692618).

References

1 W. Huang, X. Zhuang, F. S. Melkonyan, B. Wang, L. Zeng, G. Wang, S. Han, M. J. Bedzyk, J. Yu, T. J. Marks and A. Facchetti, *Adv. Mater.*, 2017, **29**, 1701706.
2 Q. Sun, J. Wang, X. Wang, J. Dai, X. Wang, H. Fan, Z. Wang, H. Li, X. Huang and W. Huang, *Nanoscale*, 2020, **12**, 16987–16994.
3 H. Wang, W. P. Lustig and J. Li, *Chem. Soc. Rev.*, 2018, **47**, 4729–4756.
4 J. Dai, O. Ogbeide, N. Macadam, Q. Sun, W. Yu, Y. Li, B. L. Su, T. Hasan, X. Huang and W. Huang, *Chem. Soc. Rev.*, 2020, **49**, 1756–1789.
5 S. Ota, A. Ando and D. Chiba, *Nat. Electron.*, 2018, **1**, 124–129.
6 H. Kim, Y. Pak, Y. Jeong, W. Kim, J. Kim and G. Y. Jung, *Sens. Actuators, B*, 2018, **262**, 460–468.
7 G. Namgung, Q. T. H. Ta, W. Yang and J. S. Noh, *ACS Appl. Mater. Interfaces*, 2019, **11**, 1411–1419.
8 H. Yuan, S. Aljneibi, J. Yuan, Y. Wang, H. Liu, J. Fang, C. Tang, X. Yan, H. Cai, Y. Gu, S. J. Pennycook, J. Tao and D. Zhao, *Adv. Mater.*, 2019, **31**, e1807161.
9 P. Li, C. Cao, Q. Shen, B. Bai, H. Jin, J. Yu, W. Chen and W. Song, *Sens. Actuators, B*, 2021, **339**, 129886.
10 S. Y. Yi, Y. G. Song, J. Y. Park, J. M. Suh, G. S. Kim, Y. S. Shim, J. M. Yuk, S. Kim, H. W. Jang, B. K. Ju and C. Y. Kang, *ACS Appl. Mater. Interfaces*, 2019, **11**, 7529–7538.
11 L. Sui, T. Yu, D. Zhao, X. Cheng, X. Zhang, P. Wang, Y. Xu, S. Gao, H. Zhao, Y. Gao and L. Huo, *J. Hazard. Mater.*, 2020, **385**, 121570.
12 H. Fu, Q. Wang, J. Ding, Y. Zhu, M. Zhang, C. Yang and S. Wang, *Sens. Actuators, B*, 2020, **303**, 127186.
13 R. Ahmad, M. S. Ahn and Y. B. Hahn, *Adv. Mater. Interfaces*, 2017, **4**, 1700691.
14 C. Hua, Y. Shang, Y. Wang, J. Xu, Y. Zhang, X. Li and A. Cao, *Appl. Surf. Sci.*, 2017, **405**, 405–411.
15 Z. Wang, C. Hou, Q. De, F. Gu and D. Han, *ACS Sens.*, 2018, **3**, 468–475.
16 L. Jun, Q. Chen, W. Fu, Y. Yang, W. Zhu and J. Zhang, *ACS Appl. Mater. Interfaces*, 2020, **12**, 38425–38434.
17 X. Liu, K. Zhao, X. Sun, C. Zhang, X. Duan, P. Hou, G. Zhao, S. Zhang, H. Yang, R. Cao and X. Xu, *Sens. Actuators, B*, 2019, **285**, 1–10.
18 S. Zhang, M. Yang, K. Liang, A. Turak, B. Zhang, D. Meng, C. Wang, F. Qu, W. Cheng and M. Yang, *Sens. Actuators, B*, 2019, **290**, 59–67.
19 Y. Guo, X. Tian, X. Wang and J. Sun, *Sens. Actuators, B*, 2019, **293**, 136–143.
20 B. Zhang, J. Liu, X. Cui, Y. Wang, Y. Gao, P. Sun, F. Liu, K. Shimanoe, N. Yamazoe and G. Lu, *Sens. Actuators, B*, 2017, **241**, 904–914.
21 G. Bae, I. S. Jeon, M. Jang, W. Song, S. Myung, J. Lim, S. S. Lee, H. K. Jung, C. Y. Park and K. S. An, *ACS Appl. Mater. Interfaces*, 2019, **11**, 16830–16837.

22 S. S. Niavol, M. Budde, A. Papadogianni, M. Heilmann, H. M. Moghaddam, C. M. Aldao, G. Ligorio, E. J. W. List Kratochvil, J. M. J. Lopes, N. Barsan, O. Bierwagen and F. Schipani, *Sens. Actuators, B*, 2020, **325**, 128797.
23 M. Sinha, S. Neogi, R. Mahapatra, S. Krishnamurthy and R. Ghosh, *Sens. Actuators, B*, 2021, **336**, 129729.
24 V. S. Bhati, M. Kumar and R. Banerjee, *J. Mater. Chem. C*, 2021, **9**, 8776–8808.
25 O. C. Compton and S. T. Nguyen, *Small*, 2010, **6**, 711–723.
26 C. Chang, W. Chen, Y. Chen, Y. Chen, Y. Chen, F. Ding, C. Fan, H. Jin Fan, Z. Fan, C. Gong, Y. Gong, Q. He, X. Hong, S. Hu, W. Hu, W. Huang, Y. Huang, W. Ji, D. Li, L.-J. Li, Q. Li, L. Lin, C. Ling, M. Liu, N. Liu, Z. Liu, K. Ping Loh, J. Ma, F. Miao, H. Peng, M. Shao, L. Song, S. Su, S. Sun, C. Tan, Z. Tang, D. Wang, H. Wang, J. Wang, X. Wang, X. Wang, A. T. S. Wee, Z. Wei, Y. Wu, Z.-S. Wu, J. Xiong, Q. Xiong, W. Xu, P. Yin, H. Zeng, Z. Zeng, T. Zhai, H. Zhang, H. Zhang, Q. Zhang, T. Zhang, X. Zhang, L.-D. Zhao, M. Zhao, W. Zhao, Y. Zhao, K.-G. Zhou, X. Zhou, Y. Zhou, H. Zhu, H. Zhang and Z. Liu, *Acta Phys.-Chim. Sin.*, 2021, **37**, 2108017.
27 K. Yang, X. Wang, H. Li, B. Chen, X. Zhang, S. Li, N. Wang, H. Zhang, X. Huang and W. Huang, *Nanoscale*, 2017, **9**, 5102–5109.
28 T. K. Dang, N. T. Son, N. T. Lanh, P. H. Phuoc, N. N. Viet, L. V. Thong, C. M. Hung, N. V. Duy, N. D. Hoa and N. V. Hieu, *J. Alloys Compd.*, 2021, **879**, 160457.
29 H. Zhang, L. Yu, Q. Li, Y. Du and S. Ruan, *Sens. Actuators, B*, 2017, **241**, 109–115.
30 M. Liu, Z. Wang, P. Song, Z. Yang and Q. Wang, *Sens. Actuators, B*, 2021, **340**, 129946.
31 V. Montes Garcia, M. A. Squillaci, M. Diez Castellnou, Q. K. Ong, F. Stellacci and P. Samori, *Chem. Soc. Rev.*, 2021, **50**, 1269–1304.
32 R. Jolly Bose, N. Illyasukutty, K. S. Tan, R. S. Rawat, M. Vadakke Matham, H. Kohler and V. P. Mahadevan Pillai, *Appl. Surf. Sci.*, 2018, **440**, 320–330.
33 J. Ma, X. Xiao, Y. Zou, Y. Ren, X. Zhou, X. Yang, X. Cheng and Y. Deng, *Small*, 2019, **15**, e1904240.
34 Q. A. Drmosh, Y. A. Al Wajih, I. O. Alade, A. K. Mohamedkhair, M. Qamar, A. S. Hakeem and Z. H. Yamani, *Sens. Actuators, B*, 2021, **338**, 129851.
35 Y. Wang, X. Meng, M. Yao, G. Sun and Z. Zhang, *Ceram. Int.*, 2019, **45**, 13150–13157.
36 J. S. Kim, H. W. Yoo, H. O. Choi and H. T. Jung, *Nano Lett.*, 2014, **14**, 5941–5947.
37 Y. Zhou, Q. Bao, L. A. L. Tang, Y. Zhong and K. P. Loh, *Chem. Mater.*, 2009, **21**, 2950–2956.
38 X. Huang, X. Zhou, S. Wu, Y. Wei, X. Qi, J. Zhang, F. Boey and H. Zhang, *Small*, 2010, **6**, 513–516.
39 K. O'Connell and J. R. Regalbuto, *Catal. Lett.*, 2015, **145**, 777–783.
40 A. Weibel, R. Bouchet, F. Boulc and P. Knauth, *Chem. Mater.*, 2005, **17**, 2378–2385.
41 F. Qu, X. Zhou, B. Zhang, S. Zhang, C. Jiang, S. Ruan and M. Yang, *J. Alloys Compd.*, 2019, **782**, 672–678.
42 P. Li, H. Zhan, S. Tian, J. Wang, X. Wang, Z. Zhu, J. Dai, Y. Dai, Z. Wang, C. Zhang, X. Huang and W. Huang, *ACS Appl. Mater. Interfaces*, 2019, **11**, 13624–13631.
43 H. Y. Lee, Y. C. Heish and C. T. Lee, *J. Alloys Compd.*, 2019, **773**, 950–954.
44 J. Hu, C. Zou, Y. Su, M. Li, X. Ye, B. Cai, E. S. W. Kong, Z. Yang and Y. Zhang, *Sens. Actuators, B*, 2018, **270**, 119–129.
45 B. I. Adamu, A. Falak, Y. Tian, X. Tan, X. Meng, P. Chen, H. Wang and W. Chu, *ACS Appl. Mater. Interfaces*, 2020, **12**, 8411–8421.
46 B. Zhang, G. Liu, M. Cheng, Y. Gao, L. Zhao, S. Li, F. Liu, X. Yan, T. Zhang, P. Sun and G. Lu, *Sens. Actuators, B*, 2018, **261**, 252–263.
47 S. Zhao, Y. Shen, F. Hao, C. Kang, B. Cui, D. Wei and F. Meng, *Appl. Surf. Sci.*, 2021, **538**, 148140.
48 M. Shafiei, J. Bradford, H. Khan, C. Piloto, W. Wlodarski, Y. Li and N. Motta, *Appl. Surf. Sci.*, 2018, **462**, 330–336.
49 X. Jiang, H. Tai, Z. Ye, Z. Yuan, C. Liu, Y. Su and Y. Jiang, *Mater. Lett.*, 2017, **186**, 49–52.
50 X. Wang, Y. Liu, J. Dai, Q. Chen, X. Huang and W. Huang, *Chem.–Eur. J.*, 2020, **26**, 3870–3876.
51 X. Wang, Z. Wang, J. Zhang, X. Wang, Z. Zhang, J. Wang, Z. Zhu, Z. Li, Y. Liu, X. Hu, J. Qiu, G. Hu, B. Chen, N. Wang, Q. He, J. Chen, J. Yan, W. Zhang, T. Hasan, S. Li, H. Li, H. Zhang, Q. Wang, X. Huang and W. Huang, *Nat. Commun.*, 2018, **9**, 3611.
52 J. Bao, S. Zeng, J. Dai, X. Wang, Q. Liu, H. Li, X. Huang and W. Huang, *Chem. Commun.*, 2021, **57**, 5590–5593.
53 H. J. Park, W. J. Kim, H. K. Lee, D. S. Lee, J. H. Shin, Y. Jun and Y. J. Yun, *Sens. Actuators, B*, 2018, **257**, 846–852.
54 J. Zha, Z. Yuan, Z. Zhou, Y. Li, J. Zhao, Z. Zeng, L. Zhen, H. Tai, C. Tan and H. Zhang, *Small Struct.*, 2021, **2**, 2100067.
55 Jyoti and G. D. Varma, *J. Alloys Compd.*, 2019, **806**, 1469–1480.
56 S. Li, Z. Wang, X. Wang, F. Sun, K. Gao, N. Hao, Z. Zhang, Z. Ma, H. Li, X. Huang and W. Huang, *Nano Res.*, 2017, **10**, 1710–1719.
57 M. Reddeppa, N. T. KimPhung, G. Murali, K. S. Pasupuleti, B. G. Park, I. In and M. D. Kim, *Sens. Actuators, B*, 2021, **329**, 129175.
58 M. S. Choi, H. G. Na, J. H. Bang, A. Mirzaei, S. Han, H. Y. Lee, S. S. Kim, H. W. Kim and C. Jin, *Sens. Actuators, B*, 2021, **326**, 128801.
59 X. Chen, S. Zhao, P. Zhou, B. Cui, W. Liu, D. Wei and Y. Shen, *Sens. Actuators, B*, 2021, **328**, 129070.
60 R. Kumar, N. Goel and M. Kumar, *ACS Sens.*, 2017, **2**, 1744–1752.
61 B. Liu, X. Liu, Z. Yuan, Y. Jiang, Y. Su, J. Ma and H. Tai, *Sens. Actuators, B*, 2019, **295**, 86–92.
62 N. D. K. Tu, J. Choi, C. R. Park and H. Kim, *Chem. Mater.*, 2015, **27**, 7362–7369.